

# Thermal stability evolution of carbon nanotubes caused by liquid oxidation

Sanja Ratkovic · Niculina Peica · Christian Thomsen ·  
Dragomir B. Bukur · Goran Boskovic

Received: 17 July 2013 / Accepted: 24 September 2013 / Published online: 23 October 2013  
© Akadémiai Kiadó, Budapest, Hungary 2013

**Abstract** Carbon nanotubes (CNTs) grown by chemical vapor decomposition of ethylene on alumina- and silica-supported Fe–Co bimetallic catalysts were examined before and after purification encompassing chemical oxidation treatment in 3 M NaOH and 3 M HNO<sub>3</sub> solutions, sequentially. Thermal properties were investigated and correlated with structural changes followed by TEM, X-ray diffraction and Raman spectroscopy characterization. Differential scanning calorimetry (DSC) and thermogravimetric analysis (TG) were employed simultaneously in the regime of TPO and TPH, in diluted flow of either O<sub>2</sub> or H<sub>2</sub>. TG revealed almost complete burning of both refined CNT samples in diluted O<sub>2</sub>, indicating the efficiency of the purification method used to remove the catalyst remains. However, different trends and significant magnitudes of changes in the heat of combustion demonstrate changes in CNTs stability after purification as a function of the catalyst support type. This is the consequence of changes in carbon type, CNTs order degree and morphology, as well as the degree of functionalization, which have their own effects on the CNTs thermal stability.

**Keywords** Thermal stability evolution · Different catalyst supports · Multi-walled carbon nanotubes · Liquid oxidation · Carbon nanotubes morphology

## Introduction

Since the discovery of carbon nanotubes (CNTs), special attention has been focused on understanding their structure, properties and use. Potential applications of CNTs significantly expanded after it was found that they can be chemically modified by functionalization of their surfaces [1]. However, CNTs may also present hazards due to flammability, and therefore, evaluation of their thermal stability during the utilization stage is very important [2]. Unfortunately, research on CNTs thermal properties is much rarer in the literature than in accounts of their synthesis [3–5], purification [6–8] and use [9–11]. According to Xu et al. [12], thermal properties of CNTs are a function of their geometric characteristics, and their stability increases with greater length for tubes with diameters in the range of 60–100 nm. For CNTs with diameters of less than 60 nm, stability decreases with increasing length. Studies of the thermal properties of different carbon-based materials have revealed lower thermal hazards for carbon composites with Al<sub>2</sub>O<sub>3</sub> powder, relative to carbon powder and commercial CNTs [13]. Likewise, addition of carbon nanotubes to epoxy matrix leads to the decrease in thermal stability of nanocomposite as an effect of thermal conductivity increase [11]. Thermal analysis of HNO<sub>3</sub>-modified multi-walled CNTs (MWCNTs) has shown higher decomposition temperature relative to as-grown material [14]. The thermal delay effect (higher onset temperature) observed after treatment in HNO<sub>3</sub> has been explained by the presence of carboxyl groups that form hydrogen bonds

---

S. Ratkovic · G. Boskovic (✉)  
Faculty of Technology, University of Novi Sad, 21000 Novi Sad,  
Serbia  
e-mail: boskovic@uns.ac.rs

N. Peica · C. Thomsen  
Institut für Festkörperphysik, Technische Universität Berlin,  
Hardenbergstraße 36, 10623 Berlin, Germany

D. B. Bukur  
Texas A&M University at Qatar, Doha, Qatar

D. B. Bukur  
Texas A&M University, College Station, TX, USA

leading to higher CNT stability. It has also been established that defect sites in the structure of the tubes have an impact on their thermal stability [15]. Defects, including edges, dangling bonds, vacancies, dislocations, etc., have different reactivity toward oxygen at higher temperatures, compared with regular tube structure. When defects are removed, by annealing at high temperature for instance, enhanced air stability is found, relative to the as-produced CNTs [15].

The aim of this research was to explore the thermal characteristics of as-produced and acid-modified carbon nanotubes, originally synthesized by the chemical vapor deposition (CVD) method over two bimetallic catalysts differing in their supports. It was expected that the different textural [16] and possibly acidic properties of the supports (alumina vs. silica) would result in the generation of tubes with different structures and that these might be further altered by means of their functionalization using acid [14, 15]. Increase in amorphous material fraction and/or defectiveness degree, which might appear due to an acid treatment of CNTs [17], may affect thermal properties in different extent in CNTs of different origin. Although the thermal stability of CNTs has been studied in the past, data on CNT behavior under regimes of temperature-programmed heating in dynamic conditions in different gas environments are scarce. Only small fraction of them is related to variety of thermal properties as function of CNTs origin (different catalysts) and purification. Of the particular interest is their behavior during heating in hydrogen, since recently much of attention has been drawn to high CNTs potential for hydrogen storage [9, 18].

The thermal properties of as-grown and purified tubes were investigated using thermogravimetric and scanning calorimetric (TG-DSC) analysis in the flow of diluted oxygen and hydrogen. Results were interpreted in terms of differences in CNTs geometry, stability, purity, and quality with regard to the presence of functional groups. Transmission electron microscopy, high-resolution transmission electron microscopy, X-ray diffraction and Raman spectroscopy were also used to characterize CNTs and further clarify the TG-DSC findings.

## Experimental

### Catalyst synthesis

Two bimetallic Fe–Co (2.5 mass % loading of each metal) catalysts were prepared by the simultaneous precipitation of equivalent masses of both metal hydroxides from the corresponding salts,  $\text{Fe}(\text{NO}_3)_3 \cdot 9\text{H}_2\text{O}$  and  $\text{Co}(\text{NO}_3)_2 \cdot 6\text{H}_2\text{O}$ , on either commercial  $\gamma\text{-Al}_2\text{O}_3$  (Ketjen Catalysts) or  $\text{SiO}_2$  (Kemika, Zagreb) supports. After aging overnight the

precipitates obtained were filtrated, washed, and dried at 110 °C for 24 h, followed by calcination in static air conditions at 600 °C for 5 h. The catalyst precursors in their oxide form were ground into powder and stored for CNTs growth.

### Carbon nanotube synthesis and purification

CNT synthesis was carried out in a home-made quartz reactor setup, as described elsewhere [19]. Catalysts in their oxide forms were reduced in situ, in a hydrogen flow, following exposure to a reaction mixture containing ethylene and nitrogen (1:1) at 700 °C for 1 h. After cooling the system in nitrogen, the content of the reactor was discharged and measured by mass. The percentage of deposit (carbon yield) was calculated, based on the reduced catalyst mass. For the sake of clarity, CNTs samples are labeled according to the catalyst support used for the tubes synthesis: CNTs-A and CNTs-S, for alumina- and silica-originated CNTs, respectively.

In order to remove the catalyst support and remaining metal particles, the raw CNT product was treated with 3 M NaOH and subsequently with 3 M  $\text{HNO}_3$  solutions for 6 h reflux at the boiling point of each, with intermediate washing. Finally, the purified carbon nanotubes were washed with distilled water and dried at 110 °C for 24 h [19].

### Characterization of products

The structure and the morphology of the as-grown and purified CNTs were characterized, using transmission electron microscopy (TEM) (Philips CM20 200 kV analytical microscope) and high-resolution transmission electron microscopy (HRTEM, JEOL-3010 300 kV).

Thermal analysis was used to study the thermal behavior of CNT samples and to ascertain their purity. Simultaneous thermogravimetric analysis (TG) and differential scanning calorimetry (DSC) was carried out, using SDT Q600 TA Instruments by means of temperature-programmed oxidation (TPO) and hydrogenation (TPH). Measurements were done in the temperature range 25–1,000 °C at a ramping rate of 10 °C  $\text{min}^{-1}$ , in a 100  $\text{cm}^3 \text{min}^{-1}$  flow of either 5 %  $\text{O}_2/\text{He}$  (TPO), or 10 %  $\text{H}_2/\text{Ar}$  (TPH). Both mixtures were prepared using high purity gases, and the flow rate was controlled by a mass flow controller integrated into the equipment.

X-ray diffraction (XRD) (Powder diffractometer Seifert MZIV with  $\text{CuK}\alpha$  radiation  $\lambda = 0.15406 \text{ nm}$ ) was used to study the crystallinity of both as-grown and purified CNTs, and the Scherrer's equation was applied to calculate the average thickness of the tube walls and therefore the mean number of graphitic planes [20].

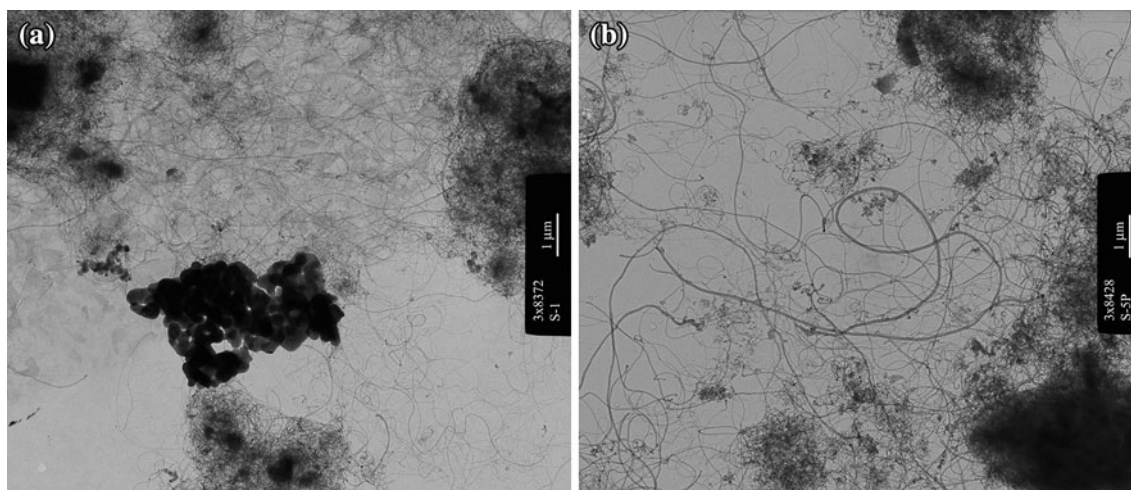


**Fig. 1** Low-magnification TEM images of as-grown CNTs over **a** Fe–Co/Al<sub>2</sub>O<sub>3</sub> and **b** Fe–Co/SiO<sub>2</sub> catalyst

Raman analyses were carried out using a LabRam HR-800 spectrometer from Horiba Jobin–Yvon. For excitation, the 532.2 nm line from a doubled-frequency Nd:YAG laser was used. The spectra were collected in backscattering geometry with a resolution of 2 cm<sup>−1</sup> and recorded with a Peltier-cooled camera [21].

## Results and discussion

Under the applied reaction conditions, the Fe–Co/Al<sub>2</sub>O<sub>3</sub> catalyst exhibited much higher activity toward CNT formation than the silica-supported one, with carbon yields of 264 and 62 %, respectively. This was confirmed by the TEM analysis revealing a larger number of entangled nanotubes in case of CNTs-A which indicates good homogeneity of the catalyst particles responsible for the efficient CNTs growth (Fig. 1a). No amorphous carbon was formed, confirming high selectivity of both catalysts and an appropriate reaction procedure which achieved equal rates of carbon-source supply and solid carbon precipitation [22].

TEM micrographs obtained at higher magnification (Fig. 2a, b) show multi-walled structures in both CNT samples regardless of used catalyst. There is no obvious difference in CNTs average thickness, products from both catalysts have diameters in the range 10–30 nm. The different locations of catalyst particles within the tubes, however, allow for speculation about diverse mechanisms of growth over the two catalysts. Thus, thin tubes with diameters about 10 nm, produced over the alumina-supported catalyst, were observed with metal particles positioned on their tops (Fig. 2a—arrows 2), indicating the “tip-growth” mechanism [23]. On the other hand, the CNTs synthesized over the silica-supported catalyst, have

metal particles only within the hollow of the tubes (Fig. 2b). In both cases, however, metal particles embedded in the interior of the tubes are probably just that part of the original metal clusters attached to the support where the growth process began [24, 25]. That is to say, at the synthesis temperature, small metal particles follow a phase transformation from solid to quasi-liquid state [26]. This enables their partial disintegration and mobility of the detached metal fraction along the emerging tube [27–29]. Once encapsulated, the particle may change its parent shape into an irregular or rod-like one, as depicted by arrow 1 in Fig. 2a and b.

Both alumina- and silica-originated CNTs were successfully purified by a “liquid oxidation” treatment [30] which efficiently eliminated catalyst remains (Fig. 3). As depicted in Fig. 3b, obtained by HRTEM, the purification treatment caused partial damage to the structure of some of the silica-originated CNTs. That can be seen on the tube positioned on the left side of the figure, by both thickness and roughness of its external walls. Furthermore, the same inner tube diameter of both tubes shown in Fig. 3b witnesses on same history of their growth; they rose on catalyst particles of the same size and by the same mechanism, resulting in tubes of same thickness [31–33]. That is to say, difference in outer diameter of two CNTs-S shown in Fig. 3b is a consequence of wall etching on some tubes during their purification.

TG, DTG and DSC profiles of as-grown and purified CNTs under TPO regimes are given in Figs. 4 and 5, while corresponding results are summarized in Table 1. Data on heat of decomposition is given both per g of sample (as measured), as well as per g of CNTs (calculated), the last accounting for omission of water and impurities from the calculation. As seen from Fig. 4, TG curves of all samples encompass profiles showing continuous mass loss, which is

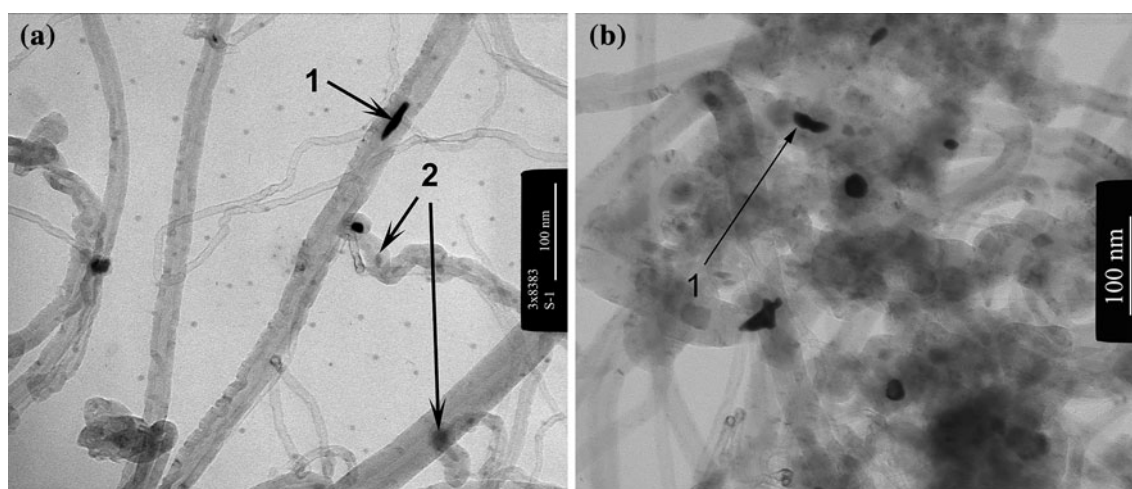


**Fig. 2** TEM image of **a** as-grown CNTs over Fe–Co/Al<sub>2</sub>O<sub>3</sub> catalyst revealing tubes with different positions and shapes of metal particles: 1-encapsulated; 2-tip metal particles and **b** as-grown CNTs over Fe–Co/SiO<sub>2</sub> catalyst with encapsulated metal particle of irregular shape

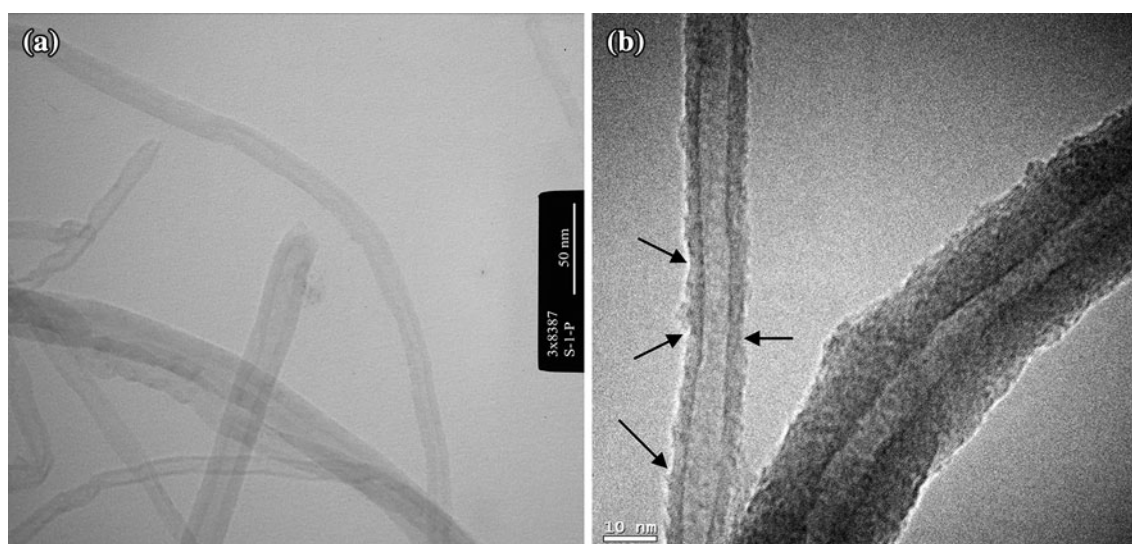


**Fig. 3** **a** TEM image of purified CNTs over Fe–Co/Al<sub>2</sub>O<sub>3</sub> catalyst and **b** HR-TEM image of purified CNTs over Fe–Co/SiO<sub>2</sub> catalyst

not in line with oxygen atoms chemisorption which has been reported to accumulate up to 50 % of original mass of single-walled nanotubes [34]. First derivative of the same curves shows oxidation maximums ranging from 610 to 630 °C, which is a temperature interval that has often been claimed for CNTs combustion to occur [15, 35]. Absence of other oxidation maximums in case of both of as-grown samples witnesses on good selectivity of CNTs synthesis, i.e., no amorphous carbon, graphitic carbon, etc.

High thermal stability of CNTs has been explained in the past by their structure defined by aromatic rather than dangling bonds [36]. However, the decomposition temperature has not been reported in the literature as a constant value but increasing one following the increase in CNTs diameter [37, 38], severity of purification conditions [17,

35, 39] and heating rate in temperature-programmed experiments [17, 39]. In addition, the fact of more reactive thinner CNTs relative to thicker ones may be overruled if impurities are present [40]. Values of heat of decomposition of CNTs presented in Table 1 are smaller compared with those usually reported in the literature, which may be accounted to the specificity of the used gas mixture, i.e., 5 %O<sub>2</sub>/He in this investigation, contrary to air, either in static [40, 41] or flow conditions [12, 34]. Almost equal values of heat of decomposition of both as-grown CNTs samples in this study, 6,738.3 and 7,006.6 J g<sub>CNTs</sub><sup>-1</sup>, obtained by omitting impurities from the calculation, speak on similar average diameter (number of walls) of both CNTs samples. However, different onset decomposition temperatures appearing in DTG profiles of as-grown CNTs

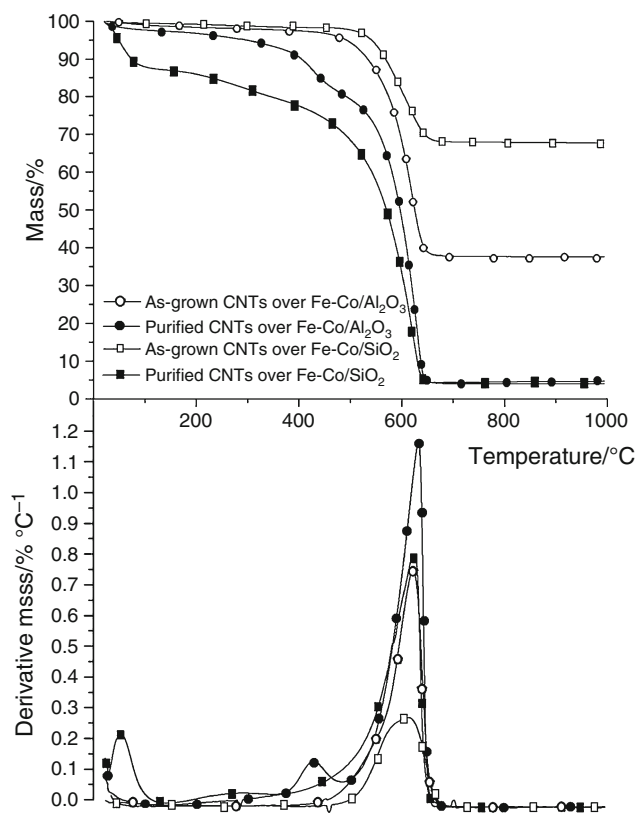


**Fig. 4** TG and DTG profiles of unpurified and purified CNTs in TPO regime

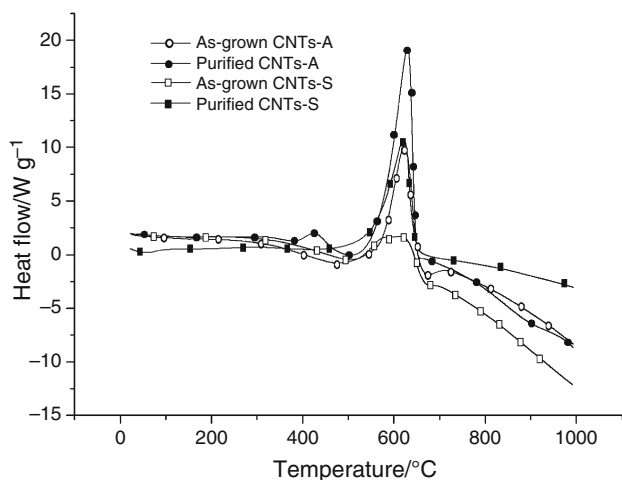


**Fig. 5** DSC profiles of unpurified and purified CNTs in TPO regime

samples may be the basis for the speculation on nonuniform samples morphology (Fig. 4). Namely, although difference in tubes diameter as a function of their synthesis history was not clarified by TEM analysis, the onset temperature shift to lower value in the case of CNTs-A compared with CNTs-S (385.6 °C relative to 465.2 °C) might indicate existence of very thin tubes in the first case,

**Table 1** Thermal analysis results obtained in TPO regime

Parameter	As-grown CNTs-A	Purified CNTs-A	As-grown CNTs-S	Purified CNTs-S
$T_o^a/^\circ\text{C}$	385.6	–	465.2	–
$T_{max}^b/^\circ\text{C}$	620.6	427.4; 631.6	611.5	622.6
Total mass loss/%	62.4	9.0; 86.4	32.2	95.9
Mass loss related to CNTs/%	60.0	76.1	30.4	75.0
Heat of sample decomposition/ $\text{J g}^{-1}$	4,043.0	6,417.4	2,138.0	4,222.0
Heat of CNTs decomposition/ $\text{J g}_{\text{CNTs}}^{-1}$	6,738.3	8,426.8	7,006.6	5,629.3
Heat of amorphous C decomposition/ $\text{J g}^{-1}_{\text{amorph C}}$	–	5,151.9	–	–

<sup>a</sup> Onset CNTs decomposition temperatures

<sup>b</sup> Maximum CNTs decomposition temperatures

<sup>c</sup> Calculated by mass loss in the CNTs combustion region

<sup>d</sup> Calculated by mass loss in the amorphous carbon combustion region

starting to decompose at lower temperature (Table 1). Lower onset temperature may also be connected to higher portion of tubes having open tips [36], but it is generally accepted view of thinner tubes having higher number of sites exposed to oxygen thus resulting in lower oxidation stability [37, 38].

Different values of mass loss of as-grown CNTs (62.4 vs. 32.2 %), indicating differences in carbon yields (Table 1), are not in line, however, with the real catalysts activity obtained by measuring the mass of catalysts before and after the synthesis. As noted, the true difference in yield is much higher, i.e., 264 vs. 62 % in favor of the alumina-based catalyst, and the discrepancy is due to the inhomogeneous samples taken for TG analysis. The problem of sample inhomogeneity can also explain highly diverse values of heat of decomposition of as-obtained CNTs measured by DSC (4,043.3 and 2,138.0  $\text{J g}^{-1}$ ), accounting for different catalyst contribution to the samples due to different yields (Fig. 5; Table 1). However, the perfect matching of mass loss data (TG) for both purified CNTs samples (~95 %) speaks in favor of the convenience of TG for checking the product purity, as well as of the applied purification method efficiency (Table 1; Fig. 4).

Samples purification led to maximal combustion temperatures increase, which can be explained by absence of catalyst originally present in both of as-grown samples (Table 1; Fig. 4). In addition, changes of heat of decomposition of purified CNTs during TPO indicate evolution of

structure as the result of purification treatment. Heat of decomposition increases from 6,738.3 to 8,426.8 J g<sub>CNTs</sub><sup>-1</sup> for CNTs-A and decreases from 7,006.6 to 5,629.3 J g<sub>CNTs</sub><sup>-1</sup> for CNTs-S upon purification (Table 1). This indicates that purification induces evolution of structure in the original CNTs, resulting in increased order degree of CNTs-A and decreased one in the case of the sample originating from the silica-based catalyst. Beside, credible values of onset temperatures of as-grown samples turned to a pretty fuzzy estimation after purification (Fig. 4). This is in particular true in the case of CNTs-A sample TG showing an additional maximum at 427.4 °C corresponding to a 9 % mass loss (Table 1). Heat of decomposition of 5,151.9 J g<sup>-1</sup>, referring to the exothermal effect at 427.4 °C implies a material having a different structure from tubes decomposing at 631.6 °C with an exothermal effect of 8,426.8 J g<sub>CNTs</sub><sup>-1</sup> (Table 1). Various forms of carbon have been shown to have different thermal resistance in air flow, i.e., 695, 645 and 420 °C for CNTs, graphite and fullerene, respectively [36]. More recent investigations attribute a peak of about 420 °C to the combustion of amorphous carbon, which appears due to purification [17, 35]. Temperatures as high as 500 and 850 °C have been claimed for amorphous carbon and graphite combustion, differing from the previously reported due to applied reaction conditions [37]. Based on results from Figs. 4, 5 and Table 1, it can be concluded that both as-grown samples went through substantial structural changes during purification, changing partly to amorphous carbon in the example of the CNTs-A sample. The observed thermal stability changes may be due to an unproportional contribution of structural imperfections, i.e., vacancies, dislocations and steps [15, 36], or the consequence of simple CNTs morphology change due to wall etching [12], both occurring during CNTs purification. However, attachment of functional groups during liquid oxidation may also induces thermal properties changes [14].

According to XRD analysis, there is a substantial change in degree of graphitization and crystallization in the case of CNTs-S upon purification (Fig. 6). As seen from the peak  $2\theta = 26.5^\circ$  corresponding to (002) graphite-like phase and by using Debye–Scherrer’s equation, the mean crystalline sizes along the tube diameter as  $L_c = 2.389$  nm may be calculated for purified CNTs-S, relative to  $L_c = 4.796$  nm for the same of the purified CNTs-A (Fig. 6b) [22]. Taking an average inter-layer distance (0.342 nm) following from Bragg’s law, a different number of graphene sheets in the tube walls can be calculated, i.e., only 7 for CNTs-S, compared with 14 in the case of CNTs-A [20]. Unfortunately, the same procedure can only partially be applied to as-grown samples since there is an interference of diffraction lines of tubes and catalyst, the last being significantly present in the case of as-grown CNTs-S (Fig. 6a). Anyhow, based on shape of XRD lines of CNTs-S before and after purification it is likely to estimate a substantial change in number of graphene sheets due to the liquid oxidation. The tubes thickness reduction is followed by decreasing of CNT-S heat of combustion as discussed above. In the case of as-grown CNTs-A, however, the same calculation showed no difference in number of graphene sheets (14) before and after purification. That is to say, the diameter of purified CNTs-S is significantly lower than it used to be in the as-grown sample, and substantially lower than the diameter of the purified tubes of another origin. This difference is the consequence of wall etching occurring during purification of the CNTs-S sample, as already was indicated in Fig. 3b. Consequently, such a process may produce defects which themselves are sites where bonding of functional groups of acidic origin is more likely to occur [42, 43]. Results of DSC and XRD in this work are both in accordance with previous findings that releasing heat during the programmed thermal treatment of CNTs decreases following their diameter decrease, but is not influenced by

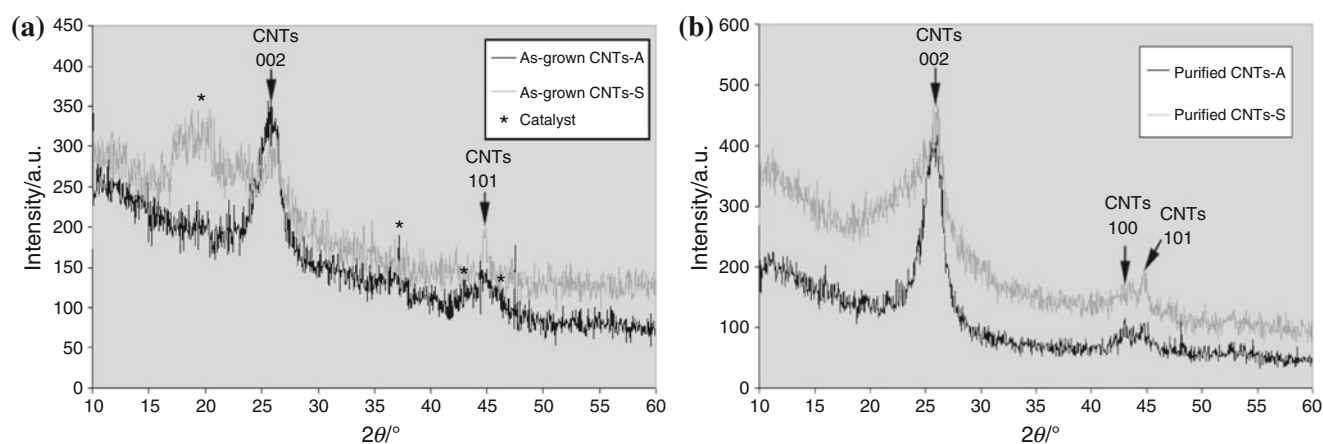


**Fig. 6** XRD profiles of **a** as-grown and **b** purified CNTs

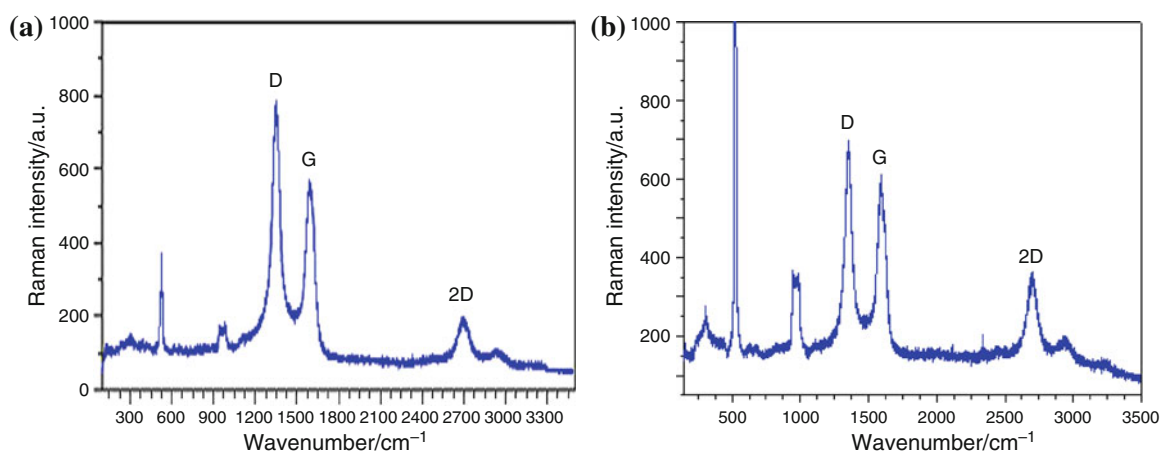


**Fig. 7** Raman spectra of **a** as-grown and **b** purified CNTs over Fe–Co/Al<sub>2</sub>O<sub>3</sub> catalyst

**Table 2** Raman spectroscopy results for as-grown and purified CNTs samples

Intensity ratio	Sample			
	CNTs-A		CNTs-S	
	As-grown	Purified	As-grown	Purified
$I_D/I_G$	1.53	1.28	1.11	1.90
$I_{2D}/I_G$	0.36	0.59	1.55	1.15

their length [12]. Chang and coworkers also found reduced value of heat of CNTs decomposition upon treatment in sulfuric acid [41]. Although they were not explicit the effect was due to diameter of CNTs decrease as a consequence of wall etching, it is, in fact, obvious from comparison of their HRTEM results of the tubes before and after acid treatment [41].

Data from Raman spectroscopy given as D band and G band, appearing about 1,350 and 1,580  $\text{cm}^{-1}$ , respectively, as well as 2D band, at about 2,700  $\text{cm}^{-1}$  [44] (Fig. 7; Table 2), are highly compatible with the CNTs thermal stability evolution observed by TPO. While D band is associated with structural defects and impurities (amorphous carbon), the G band corresponds to the stretching mode of carbon–carbon bond in the graphite plane. The 2D band is highly dispersive and is usually associated with the crystallinity degree of the nanotubes [45]. Both  $I_D/I_G$  ratio decrease and  $I_{2D}/I_G$  ratio increase in the case of CNTs-A indicate enhanced quality of the purified sample, i.e., its higher crystallinity degree upon liquid oxidation (Table 2). Beside, fairly slight intensity decrease in the D band indicates still a substantial presence of carbonaceous impurities, i.e., amorphous carbon whose appearance was above confirmed by TG. This is in line with similar findings connecting the increase in defectiveness degree with severity of acids used in purification treatment [17].

In contrast, for the CNTs-S sample both Raman indicators show the opposite trend:  $I_D/I_G$  ratio increases, indicating more structural defects formed during the purification treatment followed by the tubes functionalization, and  $I_{2D}/I_G$  value decreases, speaking on possible destruction of graphene layers during purification that leads to lower crystallinity degree (Table 2). These results of quality shift due to products purification observed by Raman are in accordance with the previous hypothesis on thermal stability evolution based on heat of decomposition of CNTs.

In order to test the quality of as-grown and the functionalization degree of purified CNTs, related samples prepared over both catalysts were subjected to thermal analysis in a TPH regime (Fig. 8; Table 3). There is a common opinion on low CNT reactivity with molecular hydrogen, even when annealed at high temperature. In the case of single-walled CNTs reactivity in hydrogen can be promoted by pressure, time of exposure, as well as the presence of catalyst remains, particularly those at the nano-scale. This resulted in both side wall hydrogenation and wall etching, occurring at 400–450 °C and above 550 °C, respectively [46]. Figure 8 displays both TG and DTG profiles in TPH conditions of as-grown and purified CNT samples of different origin. TG profiles show a mass drop amounting to 6.3 and 6.1 % for as-grown samples synthesized over alumina and silica catalysts, respectively (Table 3). The same purified samples are characterized by 10.4 and 23.1 % total mass loss, respectively. It has to be noted that presented mass losses were accommodated for different content of physically adsorbed water in the purified samples (Fig. 8). Corresponding DTG profiles indicate two different processes in as-grown samples: at the lower temperature of about 400 °C a minor reduction in catalyst remains occurs (confirmed by similar TPH profiles during the catalysts characterization, which are not shown), whereas slight hydrogenation of CNTs occurs at higher

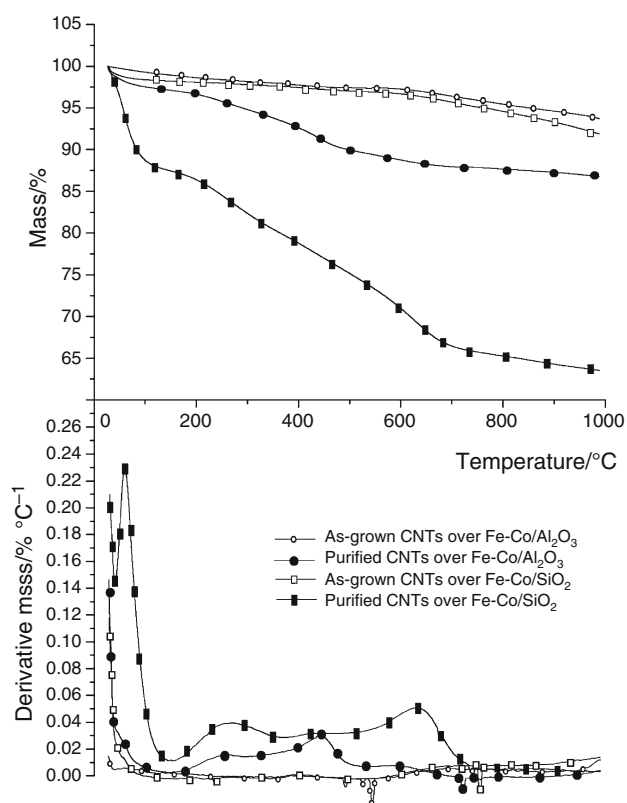


**Fig. 8** TG and DTG profiles of unpurified and purified CNTs in TPH regime

temperatures. In the case of the purified samples, however, DTG profiles are different, exhibiting three peaks in the case of the CNTs-A, and only two in the case of the tubes of another origin. Recently, during carbon nanofibers (CNFs) synthesis from ethylene, two maxima have been to assigned to hydrogenation by means of in situ evolved hydrogen: the first, occurring at temperatures as low as 200 °C, has been associated with amorphous carbon hydrogenation, and the second, at about 600 °C, attributed to hydrogenation of graphene based CNFs [47]. The last one has been shown to shift to some lower temperature depending on degree of the graphite disorder [47]. Based on our results from the TPO of purified CNTs-A, the first oxidation peak appearing at a temperature 427.4 °C was attributed to amorphous carbon combustion. Therefore, we might assume that, in the case of the same sample hydrogenation, a low temperature TPH peak of 263.2 °C corresponds to the hydrogenation of functional groups, whereas peaks of 437.9 and 582.4 °C correspond to the hydrogenation of amorphous carbon and CNTs, respectively (Fig. 8). All three peaks by their size are in line with the scenario of changes brought by purification: there are only small amount of functional groups, a substantial amount of amorphous carbon and almost no hydrogenation of thick CNTs-A which number of walls remained unchanged

**Table 3** Thermal analysis results obtained in TPH regime

Parameter	As-grown CNTs-A	Purified CNTs-A	As-grown CNTs-S	Purified CNTs-S
$T_{\max}/^{\circ}\text{C}$		263.2; 437.9; 582.4		264.8; 629.1
Total mass loss <sup>a</sup> /%	6.3	10.4	6.1	23.1
Mass loss related to functional groups/%		2.8		7.9

<sup>a</sup> Mass of water is not included

during the liquid oxidation (Raman results). In line with this reasoning, the DTG profile of the purified CNTs-S, showing absence of a middle-temperature peak, is due to the absence of amorphous carbon in that sample. Nevertheless our TPH experiment was not designed to follow the hydrogen consumption or hydrocarbons formation, based on TG and DTG profiles and peaks size we might assume a hydrogenation of functional groups at 264.8 °C and substantial hydrogenation of thin CNTs-S at 629.1 °C expressed as walls etching (Fig. 8; Table 3). A substantial mass loss at temperature above about 550 °C supports this hypothesis.

## Conclusions

Synthesis of CNTs over different catalysts (alumina and silica-based) resulted in as-grown tubes having same structural properties, as indicated by TEM, and confirmed by combustion temperatures and data of heat of combustion in regime of TPO. The efficiency of the applied liquid oxidation method in terms of purification using 3 M NaOH and subsequently 3 M HNO<sub>3</sub> solutions was confirmed by total mass losses of 95 % for both purified samples. On the other hand, the applied purification method may be too harsh for the CNTs of alumina-catalyst origin, resulting in appearance of amorphous carbon. The purification outcome is also different trends on thermal stability of the tubes grown on different catalyst, revealed as significant changes in the heat of combustion. This is partly due to changes in thickness of the silica-based catalyst CNTs as a consequence of wall etching, as confirmed by both TEM and XRD data. Raman spectroscopy data indicate further functionalization of sites formed as a consequence of wall narrowing in the case of CNTs-S and higher-order degree in the case of the CNTs of alumina-catalyst origin. Thermal analysis data of purified samples in the regime of TPH are consistent with TPO, XRD and the Raman spectroscopy results. They confirm difference in degree of functionalization, carbon nature and order degree of CNTs as a



function of their catalyst supports. In addition, a substantial mass loss at temperature above about 550 °C during TPH of silica-based CNTs indicates a possibility of additional wall attrition by means of hydrogen action.

**Acknowledgements** The financial support (Project 172059) of the Serbian Ministry of Education and Science is highly appreciated. The authors also acknowledge the TEM and HRTEM characterization by Olga Geszti, MSc, and Prof. Janos Labar of the Research Institute for Technical Physics and Materials Science, P.O. Box 49, Budapest H-1525, Hungary.

## References

1. Karousis N, Tagmatarchis N. Current progress on the chemical modification of carbon nanotubes. *Chem Rev.* 2010;110:5366–97.
2. Vignes A, Dufaud O, Perrin L, Thomas D, Bouillard J, Janes A, Vallieres C. Thermal ignition and self-heating of carbon nanotubes: from thermokinetic study to process safety. *Chem Eng Sci.* 2009;64:4210–21.
3. Nagaraju N, Fonseca A, Kónya Z, Nagy JB. Alumina and silica supported metal catalysts for the production of carbon nanotubes. *J Mol Catal A.* 2002;181:57–62.
4. Hernadi K, Kónya Z, Siska A, Kiss J, Oszkó A, Nagy JB, Kiricsi I. On the role of catalyst, catalyst support and their interaction in synthesis of carbon nanotubes by CCVD. *Mater Chem Phys.* 2002;77:536–41.
5. Dervishi E, Li Z, Biris AR, Lupu D, Trigwell S, Biris AS. Morphology of multi-walled carbon nanotubes affected by the thermal stability of the catalyst system. *Chem Mater.* 2007;19:179–84.
6. Bandow S, Rao AM, Williams KA, Thess A, Smalley RE, Eklund PC. Purification of single-wall carbon nanotubes by microfiltration. *J Phys Chem B.* 1997;101:8839–42.
7. Wang Y, Wu J, Wei F. A treatment method to give separated multi-walled carbon nanotubes with high purity, high crystallization and a large aspect ratio. *Carbon.* 2003;41:2939–48.
8. Liu YP, Wang Y, Liu Y, Li WJ, Zhou WP, Wei F. Purifying double-walled carbon nanotubes by vacuum high-temperature treatment. *Nanotechnology.* 2007;18:175704–9.
9. Nikitin A, Ogasawara H, Mann D, Denecke R, Zhang Z, Dai H, Cho K, Nilsson A. Hydrogenation of single-walled carbon nanotubes. *Phys Rev Lett.* 2005;95:225507–10.
10. De Volder MFL, Tawfick SH, Baughman RH, John Hart A. Carbon nanotubes: present and future commercial applications. *Science.* 2013;339:535–9.
11. Ciecierska E, Boczkowska A, Kurzydowski KJ, Rosca ID, Hoa SV. The effect of carbon nanotubes on epoxy matrix nanocomposites. *J Therm Anal Calorim.* 2013;111:1019–24.
12. Xu F, Sun LX, Zhang J, Qi YN, Yang LN, Ru HY, Wang CY, Meng X, Lan XF, Jiao QZ, Huang FL. Thermal stability of carbon nanotubes. *J Therm Anal Calorim.* 2010;102:785–91.
13. Chang CW, Tseng JM, Horng JJ, Shu CM. Thermal decomposition of carbon nanotube/Al<sub>2</sub>O<sub>3</sub> powders by DSC testing. *Compos Sci Technol.* 2008;68:2954–9.
14. Hsieh YC, Chou YC, Lin CP, Hsieh TF, Shu CM. Thermal analysis of multi-walled carbon nanotubes by Kissinger's corrected kinetic equation. *Aerosol Air Qual Res.* 2010;10:212–8.
15. Bom D, Andrews R, Jacques D, Anthony J, Chen B, Meier MS, Selegue JP. Thermogravimetric analysis of the oxidation of multiwalled carbon nanotubes: evidence for the role of defect sites in carbon nanotube chemistry. *Nano Lett.* 2002;2:615–9.
16. Ratkovic S, Kiss E, Boskovic G. Textural properties of carbon nanotubes upon purification by means of liquid oxidation. In: III International congress: engineering, environment and materials in processing industry, Jahorina, Book of abstracts M-11-E; 2013
17. Gallego J, Batiot-Dupeyat C, Mondragon F. Activation energies and structural changes in carbon nanotubes during different acid treatments. *J Therm Anal Calorim.* 2013;. doi:10.1007/s10973-013-2987-5.
18. Nikitin A, Li X, Zhang Z, Ogasawara H, Dai H, Nilsson A. Hydrogen storage in carbon nanotubes through the formation of stable C–H bonds. *Nano Lett.* 2008;8:162–7.
19. Ratkovic S, Kiss E, Boskovic G. Synthesis of high-purity carbon nanotubes over alumina and silica supported bimetallic catalysts. *CI&CEQ.* 2009;15:263–70.
20. Hsieh C, Lin Y, Lin J, Wei J. Synthesis of carbon nanotubes over Ni- and Co-supported CaCO<sub>3</sub> catalysts using catalytic chemical vapor deposition. *Mater Chem Phys.* 2009;114:702–8.
21. Peica N, Röhrig S, Rüdiger A, Brose K, Thomsen C, Maultzsch J. Characterization of dye molecules and carbon nanostructures by tip-enhanced Raman spectroscopy. *Phys Status Solidi B.* 2009;246:2708–12.
22. Louis B, Gulino G, Vieira R, Amadou J, Dintzer T, Galvagno S, Centi G, Ledoux MJ, Pham-Huu C. High yield synthesis of multi-walled carbon nanotubes by catalytic decomposition of ethane over iron supported on alumina catalyst. *Catal Today.* 2005;102–103:23–8.
23. Laurent C, Flahaut E, Peigney A, Rousset A. Metal nanoparticles for the catalytic synthesis of carbon nanotubes. *New J Chem.* 1998;22:1229–37.
24. Boskovic G, Ratkovic S, Kiss E, Getzi O. Carbon nanotubes purification constrains due to large Fe–Ni/Al<sub>2</sub>O<sub>3</sub> catalyst particles encapsulation. *Bull Mater Sci.* 2013;36:1–7.
25. Ratkovic S, Vujcic D, Kiss E, Boskovic G, Geszti O. Different degrees of weak metal-support interaction in Fe–(Ni)/Al<sub>2</sub>O<sub>3</sub> catalyst governing activity and selectivity in carbon nanotubes production using ethylene. *Mater Chem Phys.* 2011;129:398–405.
26. Bartholomew CH. Catalyst deactivation. *Stud Surf Sci Catal.* 1994;88:1–54.
27. Qian W, Liu T, Wang Z, Yu H, Li Z, Wei F, Luo G. Effect of adding nickel to iron–alumina catalysts on the morphology of as-grown carbon nanotubes. *Carbon.* 2003;41:2487–93.
28. Ermakova MA, Ermakov DY, Chuvilin AL, Kuvshinov GG. Decomposition of methane over iron catalysts at the range of moderate temperatures: the influence of structure of the catalytic systems and the reaction conditions on the yield of carbon and morphology of carbon filaments. *J Catal.* 2001;201:183–97.
29. Gulino G, Vieira R, Amadou J, Nguyen P, Ledoux MJ, Galvagno S, Centi G, Pham-Huu C. C<sub>2</sub>H<sub>6</sub> as an active carbon source for a large scale synthesis of carbon nanotubes by chemical vapour deposition. *Appl Catal A.* 2005;279:89–97.
30. Rinzler AG, Liu J, Dai H, Huffman CB, Rodriguez-Macias FJ, Boul PJ. Large-scale purification of single-wall carbon nanotubes: process, product, and characterization. *Appl Phys A.* 1998;67:29–37.
31. Hernadi K, Fonseca A, Nagy JB, Bernaerts D, Lucas AA. Fe-catalyzed carbon nanotube formation. *Carbon.* 1996;34:1249–57.
32. Chen P, Zhang HB, Lin GD, Hong Q, Tsai KR. Growth of carbon nanotubes by catalytic decomposition of CH<sub>4</sub> or CO on a Ni/MgO catalyst. *Carbon.* 1997;35:1495–501.
33. Cheung CL, Kurtz A, Park H, Lieber CM. Diameter-controlled synthesis of carbon nanotubes. *J Phys Chem B.* 2002;106:2429–33.
34. Illeková E, Csomorova K. Kinetics of oxidation in various forms of carbon. *J Therm Anal Calorim.* 2005;80:103–8.

35. Liu J, Harris AT. Industrially scalable process to separate catalyst substrate materials from MWNTs synthesised by fluidised-bed CVD on iron/alumina catalysts. *Chem Eng Sci.* 2009;64:1511–21.
36. Pang LSK, Saxeby JD, Chatfield SP. Thermogravimetric analysis of carbon nanotubes and nanoparticles. *J Phys Chem.* 1993; 97:6941–2.
37. McKee GSB, Vecchio KS. Thermogravimetric analysis of synthesis variation effects on CVD generated multiwalled carbon nanotubes. *J Phys Chem B.* 2006;110:1179–86.
38. Dervishi E, Li Z, Watanabe F, Xu Y, Saini V, Biris AR, Biris AS. Thermally controlled synthesis of single-wall carbon nanotubes with selective diameters. *J Mater Chem.* 2009;19:3004–12.
39. Chou YC, Hsieh TF, Hsieh YC, Lin CP, Shu CM. Comparisons of MWCNTs and acidified process by HNO<sub>3</sub> on thermal stability by DSC and TG-FTIR. *J Therm Anal Calorim.* 2010;102:641–6.
40. Sarkar S, Das PK. Non-isothermal oxidation kinetics of single- and multi-walled carbon nanotubes up to 1273 K in ambient. *J Therm Anal Calorim.* 2012;107:1093–103.
41. Chang CW, Chou YC, Tseng JM, Liu MY, Shu CM. Thermal hazard evaluation of carbon nanotubes with sulfuric acid by DSC. *J Therm Anal Calorim.* 2009;95:639–43.
42. Liu J, Rinzler AG, Dai HJ, Hafner JH, Bradley RK, Boul PJ, Lu A, Iverson T, Shelimov K, Huffman CB, Rodriguez-Macias F, Shon YS, Lee TR, Colbert DT, Smalley RE. Fullerene pipes. *Science.* 1998;280:1253–6.
43. Wiltshire JG, Khlobystov AN, Li LJ, Lyapin SG, Briggs GAD, Nicholas RJ. Comparative studies on acid and thermal based selective purification of HiPCO produced single-walled carbon nanotubes. *Chem Phys Lett.* 2004;386:239–43.
44. Ling X, Wei Y, Zou L, Xu S. The effect of different order of purification treatments on the purity of multiwalled carbon nanotubes. *Appl Surf Sci.* 2013;276:159–66.
45. Schafer DE, Wudl F, Thomas GA, Ferraris JP, Cowan DO. Apparent giant conductivity peaks in an anisotropic medium: TTF-TCNQ. *Solid State Commun.* 2007;14:347–51.
46. Talyzin AV, Luzan S, Anoshkin IV, Nasibulin AG, Jiang H, Kauppinen EI, Mikoushkin VM, Shnitov VV, Marchenko DE, Noréus D. Hydrogenation, purification, and unzipping of carbon nanotubes by reaction with molecular hydrogen: road to graphane nanoribbons. *ACS Nano.* 2011;5:5132–40.
47. Chinthajjala JK, Thakur DB, Seshan K, Lefferts L. How carbon-nano-fibers attach to Ni foam. *Carbon.* 2008;46:1638–47.